

Fractal states of the Schwinger model

E.V. Petrova,^{1,2} E.S. Tiunov,¹ M.C. Bañuls,^{3,4} and A.K. Fedorov^{1,5}

¹*Russian Quantum Center, Skolkovo, Moscow 143025, Russia*

²*Moscow Institute of Physics and Technology, Moscow Region 141700, Russia*

³*Max-Planck-Institut für Quantenoptik, Hans-Kopfermann-Str.1, 85748 Garching, Germany*

⁴*Munich Center for Quantum Science and Technology (MCQST), Schellingstr. 4, D-80799 München*

⁵*Schaffhausen Institute of Technology, Schaffhausen 8200, Switzerland*

(Dated: January 26, 2022)

The lattice Schwinger model, the discrete version of QED in 1+1 dimensions, is a well-studied test bench for lattice gauge theories. Here we study fractal properties of the Schwinger model. We reveal the self-similarity of the ground state, which allows one to develop a recurrent procedure for finding the ground-state wave functions and predicting ground state energies. We provide the results of recurrently calculating ground-state wave functions using fractal ansatz and automated software package for fractal image processing. In some parameter regimes, just a few terms are enough for our recurrent procedure to predict ground state energies close to the exact ones for several hundreds of sites. In addition, we show how the different phases present in the Schwinger model are reflected in a changing fractal structure of the wave functions. Our findings pave the way to understand the complexity of calculating many-body wave functions in terms of their fractal properties as well as to find new links between condensed matter and high-energy lattice models.

I. INTRODUCTION

Starting from its conception in 1950s, the Schwinger model [1], or quantum electrodynamics in one spatial dimension, has become a subject of intensive research. One of the reasons is that, despite being one of the simplest gauge theories, this model shares a number of non-trivial features with more complex theories, like quantum chromodynamics. The physics of the model is determined by a single dimensionless parameter m/g , which is the ratio of the particles mass m to the gauge coupling g . The Schwinger model is analytically solvable in the special cases of massless or non-interacting particles [2, 3]. However, in the general case no exact solution is known, and the model offers a challenging test bench for both analytical and numerical techniques.

Interacting quantum many-body systems are notoriously hard to describe. Analytical solutions can be applied to only particular cases, such as perturbative regimes, and, in the general case, the computational resources required for a complete numerical solution grow exponentially with the system size. Lattice gauge theories are not an exception, and it is thus natural that, specially in the last years, methods that were originally developed in the context of condensed matter physics have extended their realm to problems originating from high energy. This holds for numerical simulation techniques, such as tensor networks [4–6], and also for quantum technologies (see e.g. [7–9] for recent reviews). In particular, the Schwinger model has been object of systematic tensor network simulations [10–12]. Capabilities of quantum technologies are also under active research [7–9] starting from the pioneering experiment with a trapped-ion quantum simulator [13].

Identifying a specific structure in the state of quantum many-body systems can provide valuable insight to reduce the complexity of their description. A particular ex-

ample is the self-similar structure appearing in the wave function for certain quantum many-body problems. The qubism framework [14] has proposed a systematic way for visualizing many-body wave functions by mapping them onto two-dimensional (2D) plots. An application of qubism to condensed matter systems, such as Heisenberg or the Ising model in a transverse field, has revealed that such plots, and therefore corresponding many-body wave functions, are fractals [14]. The recursive (self-similar) nature of the plot is displayed by the fact that increasing the number of particles in the considered system reflects in an increase of pattern repetitions. Another side of the self-similarity concept is deeply related to multifractality and fractal dimensions in quantum many-body physics, which have been studied in detail for spin chains [15, 16]. One of the well-studied manifestations is the multifractality of electronic wave functions in the context of the Anderson localization [17, 18], where the wave functions are characterized by a fractal dimensionality that is different from the spatial dimensionality of the physical system [18–22]. This concept can be further extended to systems in the many-body localization phase [23–28], random matrix models [29–37], and other related physical models (for a review, see Refs. [38, 39]). An existing conjecture formulated in Ref. [15] is that multifractality is a generic property of a large class of systems with local interactions. However, very little is known about the extension of this idea for the case of systems with non-local (long-range) interactions; we note that multifractality of dipolar excitations in a random system has been considered in Ref. [40].

Here we explore the previously unobserved fractal structure in the ground state (GS) of the Schwinger model, a problem featuring nonlocal interactions. Specifically, we show the recursive nature of the ground state wave function in the strong coupling basis, which can be clearly appreciated at the level of the corresponding prob-

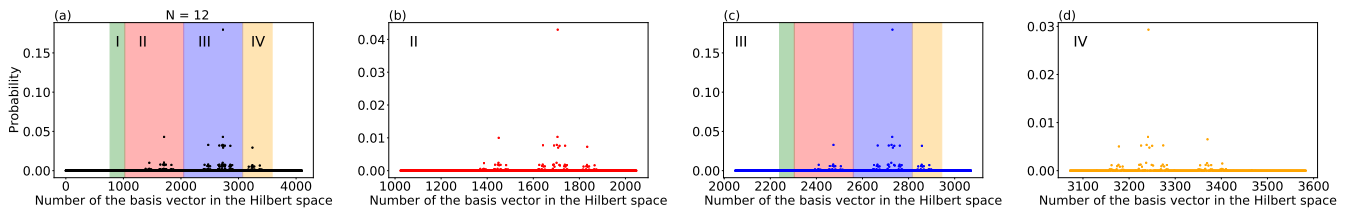


Figure 1. Fractal structure of the GS wave function. (a) the probability distribution as the function of the qubit configuration for $N = 12$ sites with four highlighted regions (green (I), red (II), blue (III), and orange (IV) regions of the distribution contain state vectors $[2^{10}, 2^{11}]$, $[2^{11}, 2^{11} + 2^{10}]$, and $[2^{11} + 2^{10}, 2^{11} + 2^{10} + 2^9]$, respectively); (b)–(d) separate plots for red, blue, and yellow regions respectively.

ability distribution, and visualized via qubism. The self-similarity as the primary feature of the fractal structure provides the possibility to construct the wave function for a larger system size starting from the exact representation for a smaller system. Here, we make use of this feature for calculating GS wave functions and their energies. We show that utilizing the recursive structure, the GS over a wide range of parameters can be written as a linear combination of a small number of terms. The accuracy of our approach can be adjusted by choosing fractal structures with higher resolution. We also show the changes in the self-similar structure when the system undergoes a phase transition.

The paper is organized as follows. In Sec. II, we discuss the Schwinger model and its mapping to the spin chain Hamiltonian. Then, in Sec. III we reveal self-similar structure of the GS wave function and introduce the fractal ansatz. Sec. IV shows how to find GS energy using self-similar properties of the model recursively. The Schwinger model in different phases is discussed in Sec. V. And, finally, we provide general outlook on the results and future perspectives in Sec. VI.

II. THE MODEL

The Schwinger model describes 1+1 quantum electrodynamics in one time and one spatial dimensions. In the continuum formulation, the Lagrangian density of the model is given by

$$\begin{aligned} \mathcal{L} &= -\frac{1}{4}F_{\mu\nu}F^{\mu\nu} + \bar{\psi}(i\mathcal{D} - m)\psi, \\ \mathcal{D} &= \gamma^\mu D_\mu = \gamma^\mu(\partial_\mu + igA_\mu(x)), \end{aligned} \quad (1)$$

ψ is the two component fermionic spinor, g is the gauge coupling, $F_{\mu\nu}$ is the electromagnetic field tensor, m is the fermionic mass, A_μ is electromagnetic two-potential, and γ_μ ($\mu=0,1$) are the Dirac matrices in 1D, which we chose as $\gamma_0 = \sigma^z$ and $\gamma_1 = i\sigma^y$.

The discrete version of the Hamiltonian representation of the model, in the physical subspace satisfying Gauss law, can be mapped to a spin chain with long range interactions [41]. To construct this representation in the most usual version, the continuum Hamiltonian is obtained

by a Legendre transformation after fixing the temporal gauge ($A_0 = 0$), and fermion fields are discretized using the Kogut-Susskind staggered formulation [42]. The resulting single-component fermionic operators are then mapped to spin 1/2 operators using a Jordan-Wigner transformation [43]. Finally, for a system with open boundary conditions, the gauge degrees of freedom can be completely eliminated using Gauss law and a gauge transformation, yielding the following Hamiltonian

$$\begin{aligned} H &= x \sum_{n=0}^{N-2} (\sigma_n^+ \sigma_{n+1}^- + \sigma_{n+1}^+ \sigma_n^-) \\ &+ \frac{\mu}{2} \sum_{n=0}^{N-1} (1 + (-1)^n \sigma_n^z) \\ &+ \sum_{n=0}^{N-2} \left(\epsilon_0 + \frac{1}{2} \sum_{l=0}^n (\sigma_l^z + (-1)^l) \right)^2 = \\ &= xV + H_{\text{diag}} \end{aligned} \quad (2)$$

where $\sigma_n^{x,y,z}$ are Pauli matrices at the site n and $\sigma^\pm = (\sigma^x \pm i\sigma^y)/2$. The Hamiltonian is parametrized by $x = 1/g^2 a^2$ and $\mu = 2m/(g^2 a)$, where a is the lattice step and ϵ_0 is the external field which we set to 0 in the rest of the paper. Here V is a hopping term and H_{diag} is the diagonal part, which include nontrivial nonlocal interaction. In such a form, the spin up on even site corresponds to the presence of a fermion, and vice versa, spin down on an odd site corresponds to the presence of an antifermion.

The Schwinger model in the spin representation preserves the global symmetries. It conserves the global charge symmetry, which in this notation implies $[\hat{H}, \hat{\sigma}_{\text{tot}}^z] = 0$, and is a consequence of the $U(1)$ gauge symmetry. Eigenstates have thus well defined charge, namely $\hat{\sigma}_{\text{tot}}^z |\psi\rangle = s_z |\psi\rangle$, where $\hat{\sigma}_{\text{tot}}^z = \sum_j \hat{\sigma}_j^z$. For even number of sites, the GS lies in the zero charge sector, or $s_z = 0$, and we will restrict the analysis to only this sector. This reduces the number of independent parameters to $\binom{N}{N/2}$. For odd number of sites, we explore only the sector $s_z = 1/2$. We provide more details about that in the next section.

III. SELF-SIMILAR STRUCTURE

OF THE GROUND STATE

We demonstrate the self-similarity of the ground state wave function by representing the state $|\Psi_N\rangle$ as a vector of size 2^N , where N is the number of sites, in the computational basis. Each element of this vector can be chosen to be real, as far as the eigenstate is nondegenerate. Fig. 1(a) illustrates the corresponding probability distribution for $N = 12$ qubits with parameters $\mu = 0.1$ and $x = 1$. A careful look at this plot can reveal four parts which are similar to the rescaled distributions for smaller number of sites. Fig. 1(b)-(d) show three out of four regions. In the figure, the green (I), red (II), blue (III), and orange (IV) regions respectively correspond to the subspaces where the first spins are projected in the following way

$$\begin{aligned} \text{I : Green} &\rightarrow P_{0011}|\Psi\rangle, \\ \text{II : Red} &\rightarrow P_{01}|\Psi\rangle, \\ \text{III : Blue} &\rightarrow P_{10}|\Psi\rangle, \\ \text{IV : Orange} &\rightarrow P_{110}|\Psi\rangle, \end{aligned} \quad (3)$$

where P_s projects the first spins of the state onto the σ_z eigenstates $|0(1)\rangle$ according to the bit string s . From the analysis of this distribution, one can see that red (II) and blue (III) region are similar to the distribution for $N - 2$ sites. The green region (I) contains the distribution for $N - 4$ qubits, while the orange (IV) resembles the flipped distribution for the state of $N - 3$ sites. The flipped distribution comes from original one by exchanging 0 and 1 in a spin configuration. To obtain some of the regions, the distribution for smaller number of qubits is scaled by some factor, which we further refer to as *weight*. The peculiar property of self-similarity dictates that these weights should be the same for any number of sites. We find that values of weights depend on the number of qubits for small systems, but they become constant after some system size, as shown in Fig. 2 (see also Supplementary Information Fig. S1). The same situation takes place for conventional fractals: an ideal fractal is self-similar to itself at any scale, while this property is valid only approximately for real structures.

The self-similar structure is not just a beautiful peculiarity, but also a way to a compact ansatz based on that structure. The most compact version of such an ansatz is as follows:

$$\begin{aligned} |\Psi_N^A\rangle = & W_{0011}^N |0011\rangle |\Psi_{N-4}\rangle + W_{01}^N |01\rangle |\Psi_{N-2}\rangle + \\ & + W_{10}^N |10\rangle |\Psi_{N-2}\rangle + W_{110}^N |110\rangle \hat{T} |\Psi_{N-3}\rangle \end{aligned} \quad (4)$$

where $\hat{T} = \otimes_k \hat{\sigma}_k^x$ is the bit flipping operator. Eq. (4) explicitly expresses the approximation of the GS for N sites in terms of ground states for smaller systems. Each term in the linear combination consists of two factors: a set of initial spins in a fixed configuration in the computational basis, and a (sometimes flipped) ground state of a smaller dimension. To preserve the zero total charge for even number of sites in Eq. (4), the GS for odd number

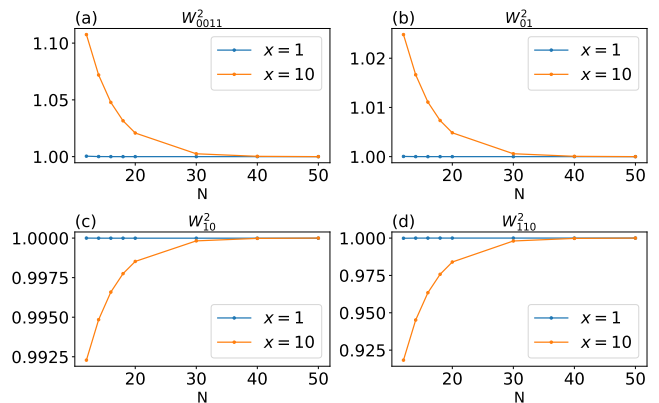


Figure 2. The behaviours of weights squared ($W_s^2 = ||P_s|\Psi\rangle||^2$) as a function of the number of sites, N , for $x = 1$ and $x = 10$, $\mu = 0.1$ normalized to the its maximum absolute value.

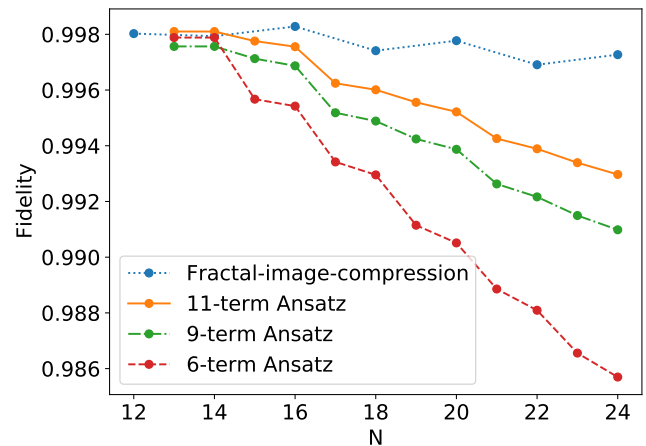


Figure 3. The fidelity, $\mathcal{F} = |\langle \Psi_{\text{exact}} | \Psi \rangle|^2$, where Ψ_{exact} is the exact GS obtained by exact diagonalization and Ψ is our prediction, is shown as a function of the system size (N) for parameters $x = 1, \mu = 0.1$. For the fractal-image compression algorithm we use qubism representation of the wave function and apply compression-decompression algorithm, decompressing it into the picture of the interested size. For the recursion algorithm we use 6, 9, 11-term ansatzes which includes 9, 11 terms respectively and depends on the distributions for $N - 2, N - 3, N - 4, N - 5, N - 6, N - 7, N - 8$ qubits. The recurrent procedure for obtaining wave functions is approximate, so the accumulation of errors leads to the decrease in the fidelity.

has to lie in the $+1/2$ sector (1 is spin up and 0 is spin down). The coefficients W denote scaling weights, which include the relative 0 or π phase.

The ansatz (4) is compact and presents only a first level of approximation. To obtain a more accurate approximation, we need to increase the number of terms in the ansatz, by taking into account more parts of the distribution. Table I shows the extended ansatzes with 4, 6, 9, and 11 terms. Each column in the table shows the terms that are considered as the basis for that particular

11-term	9-term	6-term	4-term
$ 001011\rangle \Psi_{N-6}\rangle$	$ 001011\rangle \Psi_{N-6}\rangle$	$ 001011\rangle \Psi_{N-6}\rangle$	
$ 0011\rangle \Psi_{N-4}\rangle$	$ 0011\rangle \Psi_{N-4}\rangle$	$ 0011\rangle \Psi_{N-4}\rangle$	$ 0011\rangle \Psi_{N-4}\rangle$
$ 01\rangle \Psi_{N-2}\rangle$	$ 01\rangle \Psi_{N-2}\rangle$	$ 01\rangle \Psi_{N-2}\rangle$	$ 01\rangle \Psi_{N-2}\rangle$
$ 10001011\rangle \Psi_{N-8}\rangle$			
$ 100011\rangle \Psi_{N-6}\rangle$	$ 100011\rangle \Psi_{N-6}\rangle$		
$ 1001\rangle \Psi_{N-4}\rangle$	$ 1001\rangle \Psi_{N-4}\rangle$	$ 10\rangle \Psi_{N-2}\rangle$	$ 10\rangle \Psi_{N-2}\rangle$
$ 1010\rangle \Psi_{N-4}\rangle$	$ 1010\rangle \Psi_{N-4}\rangle$		
$ 10110\rangle \hat{T} \Psi_{N-5}\rangle$	$ 10110\rangle \hat{T} \Psi_{N-5}\rangle$		
$ 1011100\rangle \hat{T} \Psi_{N-7}\rangle$			
$ 110\rangle \hat{T} \Psi_{N-3}\rangle$	$ 110\rangle \hat{T} \Psi_{N-3}\rangle$	$ 110\rangle \hat{T} \Psi_{N-3}\rangle$	$ 110\rangle \hat{T} \Psi_{N-3}\rangle$
$ 11100\rangle \hat{T} \Psi_{N-5}\rangle$	$ 11100\rangle \hat{T} \Psi_{N-5}\rangle$	$ 11100\rangle \hat{T} \Psi_{N-5}\rangle$	

Table I. Each column consists of basis elements which define ansatzes with 4, 6, 9, and 11 terms. The bit string defines a fixed state for the first few qubits from the beginning, $|\Psi_M\rangle$ is the GS for M qubits.

approximation. These bases are inspired by our empirical observation of self-similar structure for small number of qubits. We show the detailed derivation of the 6, 9, and 11-term ansatzes in Supplementary Information.

The fractal ansatz better approximates the true quantum state if weights do not change with the system size. We indeed observe that increasing the system size we get closer to the ideal fractal, in which weights are the same for different scales.

In the case $x = 1$ and $\mu = 0.1$, exact diagonalization of small systems is enough to obtain the behaviour of the weights until convergence. For different parameters x and μ , MPS calculations for different number of qubits demonstrate that weights actually also converge (see Supplementary Information).

The qubism framework [14], which establishes the specific mapping between many-body quantum states and 2D plots, provides an alternative way to capture the self-similarity of the model. For even number of sites, qubism maps the wave function onto a square image of size $2^{N/2} \times 2^{N/2}$. Each pixel of the image represent the absolute square of the amplitude for a single basis state. The order of the pixels in the image is such that each row corresponds to one of the $2^{N/2}$ configurations of the spins on even positions, while each column corresponds to a given configuration of the odd spins. For example, a four qubit state corresponds to a 4 by 4 image in the qubism representation, see Fig. 4. We illustrate the fractal structure of the GS wave functions for different values of the system size in Fig. 5.

Since the qubism framework provides a way to look at a state as an image, one can use a large variety of computer graphics software for obtaining a compact image representation. Having this representation, one can decompress the image into a grey scale image of an arbitrary size, thus generating a distribution for a larger system. The particular class of such algorithms is fractal-image-compression [44]. The idea is to find transformations which scale larger parts into smaller parts (compression) and vice versa (decompression), such that the parts after the transformation are similar to the corresponding piece of the original image. Specifically, we use the

0000	0001	0100	0101
0010	0011	0110	0111
1000	1001	1100	1101
1010	1011	1110	1111

Figure 4. Qubism representation for a 4 qubit state, in which bitstrings denote qubit configurations of a state. Each rectangle represents a pixel, which value is the corresponding probability to the power of 0.2.

simplest fractal-compression-decompression package [45], which implements segmentations, compression, and decompression of images. Post processing is also required. After the decompression step, we apply a mask that nullifies all the amplitudes that violates the total spin conservation and then normalize the whole state.

In order to compare various algorithms for recurrent state construction, we plot the fidelity of the reconstructed ground state as a function of the system size in Fig. 3. The starting point is chosen to be the GS for 12 qubits obtained by exact diagonalization. Solid, dashed-dotted and dashed lines depict fractal ansatzes with 11, 9 and 6 terms, respectively, while the dotted curve shows the results for the image compression algorithm. The 11-term ansatz shows superior results, as it is a more accurate approximation compared to the 9 and 6-term ansatzes. At the same time, we observe that both fractal methods give a bigger drop in the fidelity with the system size than the computer graphics algorithm. This algorithm splits the state into a larger number of parts. We assume that this fact leads to higher fidelity than fractal ansatzes. Another important problem which is worth to be discussed is the error of fractal method. This comes from two sources. The GS lies in a particular charge sector. Different fractal ansatzes cover different parts of that sector. If the coverage is less, the error is

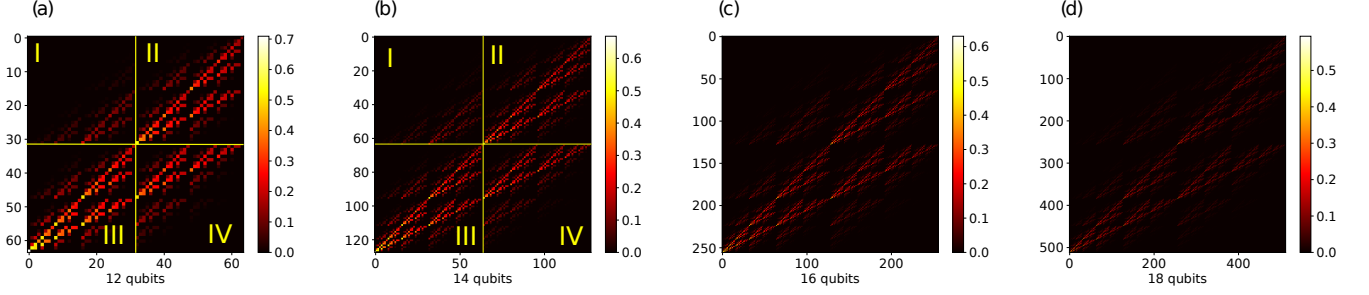


Figure 5. Fractal structure of the GS wave functions of the model in the qubism representation for (a) $N = 12$, (b) $N = 14$, (c) $N = 16$, and (d) $N = 18$ qubits and parameters $x = 1$, $\mu = 0.1$. Regions II and III for 12 and 14 qubit distributions coincide with regions on the Fig. 1, I and IV regions extend that of the Fig. 1. The qubism shows the main property: increase of the image resolution reflects in an increase of self-replicating structures.

greater. The second source is how well the fractal structure of the ansatz matches that of the real state. The error related to the coverage can be quantified by summing squared values of weights, which should be one for a perfect ansatz (see Supplementary Information, Fig S2). In our case, the 6-term ansatz has the smallest loss of pro. However, 9- and 11-term ansatzes provide better approximation for large N (higher fidelity on Fig. 3), since their structures are better fitted to the ideal GS.

We would like to note that the same procedure can be realized for distributions associated with different values of the parameters of the model. The explored fractal property is also preserved in different bases (see Supplementary Information, Fig. S3.)

IV. GROUND-STATE ENERGY

Assuming a fractal ansatz, we can search for the GS in the subspace generated by the terms included in the wave function. In particular, ansatz (4) defines the four dimensional subspace spanned by the following basis: $\{|0011\rangle|\Psi_{N-4}\rangle, |01\rangle|\Psi_{N-2}\rangle, |10\rangle|\Psi_{N-2}\rangle, |110\rangle T|\Psi_{N-3}\rangle\}$. For extended, more accurate ansatzes, we need to construct subspaces of larger dimensions, as specified by the terms in Table I. For simplicity, here we show explicitly the procedure for only the simplest ansatz (4), while details about the extended ansatzes can be found in the Supplementary Material.

The reduced Hamiltonian projected into the subspace generated by the basis can be represented using formula $(\hat{H}_N^R)_{ij} = \langle\phi_i|\hat{H}|\phi_j\rangle$ where ϕ_i are the basis vectors. Thus, the reduced Hamiltonian looks as follows:

$$\hat{H}_N^R = \begin{pmatrix} E_{N-4} + 3 + 2\mu & xA_N & 0 & 0 \\ xA_N & E_{N-2} + 1 + 2\mu & xB_N & 0 \\ 0 & xB_N & E_{N-2} & xC_N \\ 0 & 0 & xC_N & E_{N-3} + 1 + 2\mu \end{pmatrix} \quad (5)$$

where E_M is the ground state energy for size M , and we have introduced the overlaps $A_N = \langle 01|\langle\Psi_{N-4}|\Psi_{N-2}\rangle$,

$B_N = \langle\Psi_{N-2}|\Psi_{N-2}\rangle$ and $C_N = \langle 1|\langle\hat{T}\Psi_{N-3}|\Psi_{N-2}\rangle$. Diagonal elements consist of GS energies for the previous system sizes, since the Hamiltonian for N spins expressed in terms of Hamiltonians for $N-4$, $N-2$, and $N-3$ spins. The additional constants on the diagonal come from nonlocal and mass terms. The nondiagonal elements are defined by the hopping part of the Hamiltonian acting on first fixed qubits. We can compute these overlaps by noticing that A_N can be expressed in terms of a weight from a smaller system size and C_N as a recurrent function as follows:

$$\begin{aligned} A_N &= \langle 01|\langle\Psi_{N-4}|\Psi_{N-2}\rangle = W_{01}^{N-2}, \\ B_N &= \langle\Psi_{N-2}|\Psi_{N-2}\rangle = 1, \\ C_N &= \langle 1|\langle\hat{T}\Psi_{N-3}|\Psi_{N-2}\rangle = f_{N-2}, \\ f_{N-2} &= W_{10}^{N-2}(W_{10}^{N-3}f_{N-4} + W_{110}^{N-3}W_{01}^{N-4}) \\ &\quad + W_{110}^{N-2}W_{01}^{N-3}. \end{aligned}$$

The smallest eigenvalue of matrix (5) gives the estimation of the GS energy and the corresponding eigenvector provides values of weights $(W_{0011}^N, W_{01}^N, W_{10}^N, W_{110}^N)$ for N qubits. Starting from the exact solution for small systems from ED, the ground state energy estimation can be obtained recursively for any system size. We refer this method to as ansatz Diagonalization (AD). The algorithm for finding the ground state energy is expressed in the following steps.

- **Step 0.** Find initial weights, overlaps and GS energies using ED up to N_0 number of spins.
- **Step 1.** Construct the reduced Hamiltonian matrix for $N_0 + 1$ spins in the basis generated by the fractal ansatz.
- **Step 2.** Find the minimal eigenvalue and corresponding eigenvector of that matrix for $N_0 + 1$ spins.
- **Step 3.** Save the weights, which are elements of the minimal eigenvector, and the minimal eigenvalue, calculate overlaps from the weights for $N_0 + 1$ spins.
- **Step 3.** Repeat from step 1 increasing the initial system size $N_0 \rightarrow N_0 + 1$.

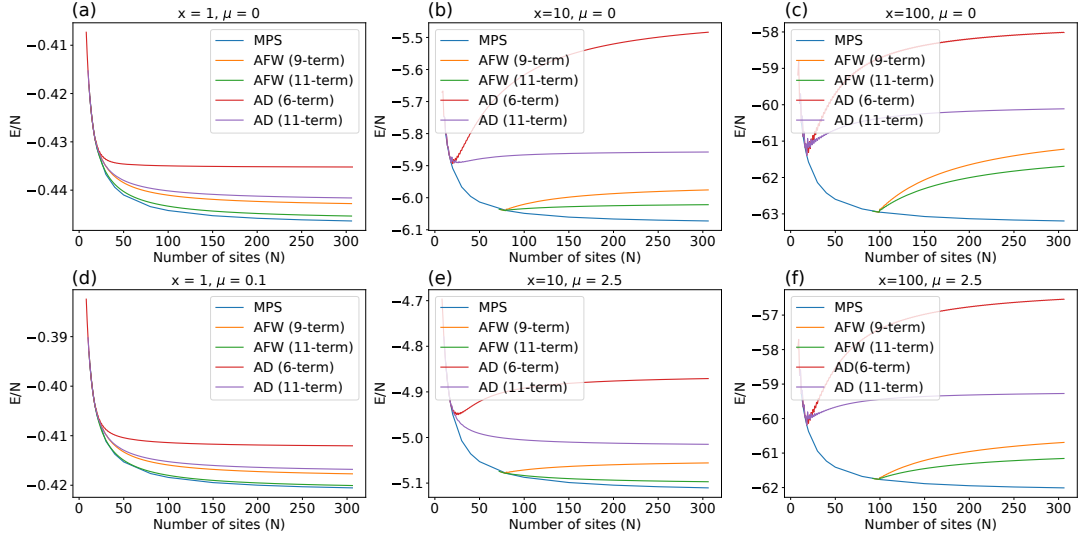


Figure 6. GS energy estimations with the number of sites for different x and μ . Results are obtained using MPS algorithm, ansatz with fixed weights (AFW) and ansatz diagonalization procedure (AD), both AD and AFW contain either 6,9 or 11 terms.

For each step of the algorithm above, we calculate weights recursively. However, in general case, the weights converge to constants starting from some system size which depends on the parameters x and μ (see Supplementary information, Fig. S1). This system size lies in the range accessible to ED calculations only for small x and large μ . When the system approaches to the continuum limit (large x) the weight convergence happens much further than in the previous case. Thus, the only way to calculate weights at that point is to utilise MPS calculations. In any case, we can start from this particular point, and repeat procedure of calculating energy, assuming that weights are fixed. Then the simple formula for the energy is the following:

$$\begin{aligned}
 E_N = & (W_{0011})^2(E_{N-4} + 3 + 2\mu) + \\
 & + (W_{01})^2(E_{N-2} + 1 + 2\mu) + (W_{10})^2 E_{N-2} + \\
 & + (W_{110})^2(E_{N-3} + 1 + 2\mu) \\
 & + 2W_{0011}W_{01} \langle 01 | \langle \Psi_{N-4} | \Psi_{N-2} \rangle + \\
 & + 2W_{01}W_{10} \langle \Psi_{N-2} | \Psi_{N-2} \rangle + \\
 & + 2W_{10}W_{110} \langle 1 | \langle \hat{T} \Psi_{N-3} | \Psi_{N-2} \rangle
 \end{aligned} \tag{6}$$

where E_N is the mean value of the Hamiltonian averaged over fractal ansatz (4) for N qubits. Here we assume that values of the weights are the converged ones, $W_s := \lim_{N \rightarrow \infty} W_s^N$. The state preserves its self-similar structure since the weights converge with the system size. We can deduce from this fact that overlaps also become constants along with weights.

The procedure of finding the GS energy using the ansatz with Fixed Weights (AFW) consists of the following steps.

- **Step 0.** Choose initial system size N_0 by observing the behaviour of the weights with the number

of spins. At the starting point, weights have to converge.

- **Step 1.** Calculate the weights, overlaps and energies up to N_0 spins according to the ansatz using exact diagonalization or MPS approach.
- **Step 2.** Calculate energy using formula (6) for $N_0 + 1$ system size.
- **Step 3.** Save energy for $N_0 + 1$ spins and repeat from the step 2 by reassigning initial system size $N_0 \rightarrow N_0 + 1$.

The procedure of calculating energy can be improved by including more terms (Table I). We provide more details about that in the Supplementary information.

The results of our GS energy estimation are presented in Fig. 6. We observe that, in general, ansatzes with larger number of terms lead to a better approximation of the GS energy. Such behavior is valid for all dependencies in the Fig. 6. Our fractal algorithms demonstrate the best performance for larger lattice steps (small x) and bigger masses μ . AFW methods show slightly better energy approximations compared to the AD algorithm. However, the starting point of AFW procedure demands MPS calculations for $x = 10, 100$, while the only information needed to launch AD algorithm is obtained by ED.

We observe two different energy behaviours on Fig. 6, where some curves decrease monotonically, while others [Fig. 6(b,c,f) and red and orange curves of on Fig. 6(e)] exhibit non-monotonical behaviour. We interpret this behaviour as indicative of an insufficient ansatz, which needs to include more terms. As one can see from Fig. 6(d), predictions of the GS energy given by the AD 11-term ansatz are very close to the results of MPS even for large enough $N \approx 300$ number of sites.

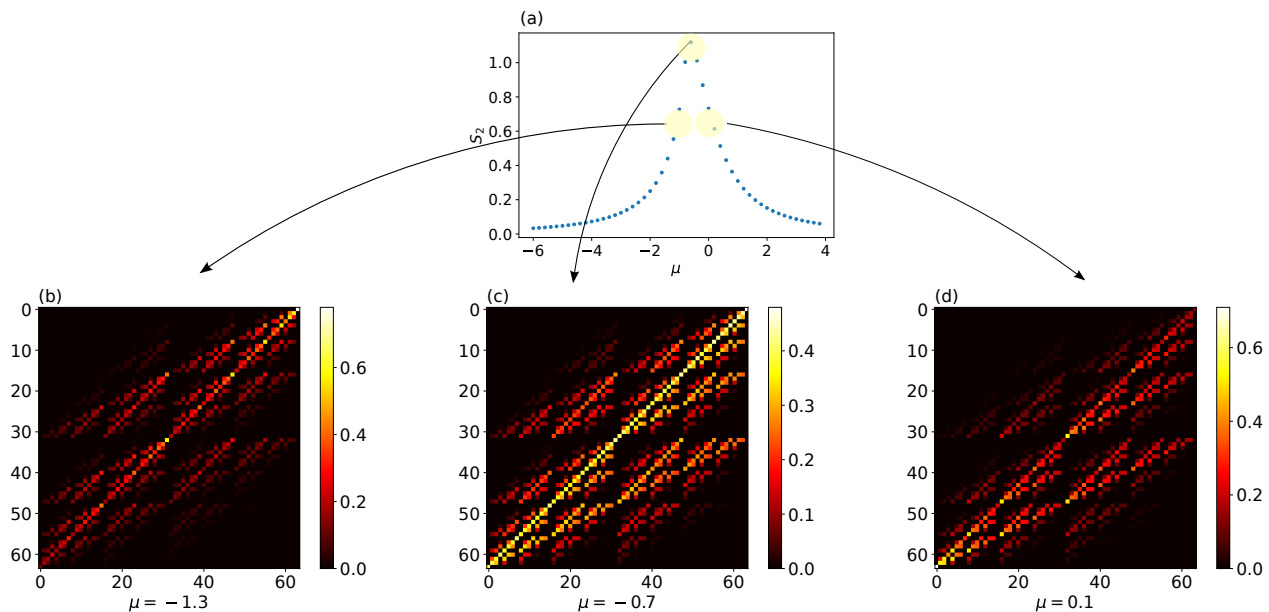


Figure 7. The phase transition in the system of $N = 12$ qubits at $x = 1$ and different μ is illustrated in the qubism framework.

Our method provides an upper bound on the energy of the GS, as the procedures are variational. There are two related arguments for the deviation between our ansatz and MPS estimations. First, different regions of the GS do not perfectly coincide with wave functions for smaller dimensions. Second, some amplitudes, which are not covered by our ansatz, can contribute to the GS energy. However, our estimations do not diverge with the growing system size even in the presence of discrepancies described above.

V. FRACTAL STRUCTURE IN DIFFERENT PHASES

At a certain value of the background field (corresponding to $\epsilon_0 = 1/2$ in the lattice formulation) and at the critical mass $(m/g)_c \approx 0.33$, the Schwinger model exhibits a second order phase transition belonging to the Ising universality class [46, 47]. In the zero charge sector, it is possible to unitarily transform the Hamiltonian such that $\epsilon_0 \rightarrow \epsilon_0 - 1/2$ and $\mu \rightarrow -\mu$, so that the same critical behaviour can be observed at zero background field for a negative mass [48]. This phenomenon has in fact been object of recent variational quantum simulation experiments [49, 50].

In terms of the spin representation, we can understand the different nature of both phases by comparing the ground states in the limits $\mu \rightarrow \pm\infty$. For $\mu \gg 0$, the energetically favoured configuration is $|0101\dots 01\rangle$, corresponding to a full filling of fermions and antifermions, while for $\mu \ll 0$, the ground state is empty, which corresponds to $|1010\dots 10\rangle$.

To detect the transition, we can use the Renyi en-

tropy [49, 51]

$$S_2 = \frac{\log(\sum_i P_i^2)}{\log M} \quad (7)$$

where P_i are probabilities of each basis state in the wave function, and M is the dimension of the Hilbert space. At $x = 1$, the value of μ corresponding to the (negative) critical mass is $\mu \sim -0.7$. We show in Fig. 7(a) the value of the Renyi entropy as a function of μ for a system size $N = 12$.

The fractal structure of the wave function also essentially changes across the critical point. The structure of the qubism representation is common for both phases but reflected around diagonal and antidiagonal in the qubism representation Fig. 7. This two reflections correspond to the exchanging 0 and 1 in spin configurations. The top right pixel is the brightest one in the phase where $\mu < -0.7$. This pixel corresponds to the spin configuration $|0101\dots 01\rangle$ which is the vacuum of 1D QED model. The situation in the other phase is the opposite. The brightest one is the bottom left pixel, which is the full filling of electrons on a lattice ($|1010\dots 10\rangle$ spin configuration).

VI. CONCLUSION AND OUTLOOK

Specific properties of quantum many-body systems that potentially could help to overcome the curse of dimensionality challenge in their simulation are of enormous interest. Finding fractal structure for various many-body Hamiltonians within the qubims representation [14] and the conjecture by Atas and Bogomolny [15] that the multifractality is essential for 1D spin chains

with local interaction have formed the comprehensive theoretical background in this domain. In this work, we have expanded the fractal property for the ground state of the Schwinger model featuring non-local interaction. Moreover, we have used the fractal structure to introduce the representation of the wave function in terms of the system's states for smaller number of sites. Despite the simplicity of the approach, we have demonstrated that our fractal ansatz gives very accurate results for both the ground-state wave function, where we compared our results with the exact diagonalization up to 24 sites, and the ground state energy. In the latter case, we see our predictions are very close (accuracy 99.75%) to the results of the state-of-the-art MPS method even for large enough ($N \approx 300$) number of sites in the case of big lattice step ($x = 1$). We note that the fractal ansatz is computationally efficient (all the results are obtained with the use of modest computational resources of PC) and has the feature of controlling its accuracy by increasing the number of terms.

Many paths for expanding our approach can be envisaged in the near future. First of all, we expect that the fractal ansatz can be used to describe a broader class of systems, for example, in condensed matter. It is interesting to reveal where the fractal property preserves for systems with other types of non-local character of interactions. Specifically, it seems to be promising to establish relations to fractal states of quantum matter, such as fractal spin liquids [52].

In this work, we have stressed on the analyzing the fractal properties of wave functions themselves. However, the fractal properties may be reflected also in their

MPS representation. One may expect that using the self-similar properties discussed in this paper could be beneficial to work with such representations, e.g. in terms of the reduction of computational resources.

Finally, as we have shown there are opportunities to use automatic packages for fractal analysis algorithms in order to make predictions about the system structure at larger sizes. We have implemented the proof-of-principle demonstration, whereas more detailed analysis of the potential of such tools in quantum many-body physics is required. For example, a way to use MPS for image compression has been suggested [53] and string-bond states, which are deeply related to neural network quantum state representations, has demonstrated a potential for classical machine learning applications [54]. We then expect that new interfaces between image compression tools and representations for quantum many-body systems may be found with the help of fractal ansatzes).

ACKNOWLEDGEMENTS

M.C.B. thanks S. Kühn for discussions about the phase structure of the model. A.K.F. thanks V. Gritsev and A. Garkun for insightful comments. E.V.P., E.S.T., and A.K.F. thank the support by the Russian Science Foundation Grant No. 20-42-05002 (studying the fractal ansatz) and the Russian Roadmap on Quantum Computing (calculating on ground-state energies). M.C.B. was partly funded by the Deutsche Forschungsgemeinschaft (DFG, German Research Foundation) under Germany's Excellence Strategy – EXC-2111 – 390814868.

-
- [1] J. Schwinger, *Phys. Rev.* **82**, 914 (1951).
 - [2] J. Schwinger, *Phys. Rev.* **128**, 2425 (1962).
 - [3] D. Crewther and C. Hamer, *Nuclear Physics B* **170**, 353 (1980).
 - [4] U. Schollwöck, *Annals of Physics* **326**, 96 (2011).
 - [5] F. Verstraete, V. Murg, and J. Cirac, *Advances in Physics* **57**, 143 (2008).
 - [6] R. Orús, *Annals of Physics* **349**, 117 (2014).
 - [7] E. Zohar, *Philosophical Transactions of the Royal Society A: Mathematical, Physical and Engineering Sciences* **380**, 20210069 (2022).
 - [8] M. C. Bañuls, R. Blatt, J. Catani, A. Celi, J. I. Cirac, M. Dalmonte, L. Fallani, K. Jansen, M. Lewenstein, S. Montangero, C. A. Muschik, B. Reznik, E. Rico, L. Tagliacozzo, K. Van Acoleyen, F. Verstraete, U.-J. Wiese, M. Wingate, J. Zakrzewski, and P. Zoller, *The European Physical Journal D* **74**, 165 (2020).
 - [9] M. C. Bañuls and K. Cichy, *Reports on Progress in Physics* **83**, 024401 (2020).
 - [10] M. C. Bañuls, K. Cichy, J. I. Cirac, and K. Jansen, *Journal of High Energy Physics* **2013**, 158 (2013).
 - [11] K. Zapp and R. Orús, *Phys. Rev. D* **95**, 114508 (2017).
 - [12] N. Butt, S. Catterall, Y. Meurice, R. Sakai, and J. Unmuth-Yockey, *Phys. Rev. D* **101**, 094509 (2020).
 - [13] E. A. Martinez, C. A. Muschik, P. Schindler, D. Nigg, A. Erhard, M. Heyl, P. Hauke, M. Dalmonte, T. Monz, P. Zoller, and R. Blatt, *Nature* **534**, 516 (2016).
 - [14] J. Rodríguez-Laguna, P. Migdał, M. I. Berganza, M. Lewenstein, and G. Sierra, *New Journal of Physics* **14**, 053028 (2012).
 - [15] Y. Y. Atas and E. Bogomolny, *Phys. Rev. E* **86**, 021104 (2012).
 - [16] Y. Y. Atas and E. Bogomolny, *Philosophical Transactions of the Royal Society A: Mathematical, Physical and Engineering Sciences* **372**, 20120520 (2014).
 - [17] P. W. Anderson, *Phys. Rev.* **109**, 1492 (1958).
 - [18] F. Evers and A. D. Mirlin, *Rev. Mod. Phys.* **80**, 1355 (2008).
 - [19] M. Janssen, *Physics Reports* **295**, 1 (1998).
 - [20] A. D. Mirlin, *Physics Reports* **326**, 259 (2000).
 - [21] A. D. Mirlin, Y. V. Fyodorov, A. Mildnerberger, and F. Evers, *Phys. Rev. Lett.* **97**, 046803 (2006).
 - [22] A. De Luca, B. L. Altshuler, V. E. Kravtsov, and A. Scardicchio, *Phys. Rev. Lett.* **113**, 046806 (2014).
 - [23] F. Wegner, *Zeitschrift für Physik B Condensed Matter* **44**, 9 (1981).
 - [24] B. L. Altshuler, V. E. Kravtsov, and I. V. Lerner, *JETP Letters* **43**, 441 (1986).

- [25] C. Monthus, *Journal of Statistical Mechanics: Theory and Experiment* **2016**, 073301 (2016).
- [26] M. Serbyn, Z. Papić, and D. A. Abanin, *Phys. Rev. B* **96**, 104201 (2017).
- [27] N. Macé, F. Alet, and N. Laflorencie, *Phys. Rev. Lett.* **123**, 180601 (2019).
- [28] G. De Tomasi, I. M. Khaymovich, F. Pollmann, and S. Warzel, *Phys. Rev. B* **104**, 024202 (2021).
- [29] A. D. Mirlin, Y. V. Fyodorov, F.-M. Dittes, J. Quezada, and T. H. Seligman, *Phys. Rev. E* **54**, 3221 (1996).
- [30] A. Telcs and N. Wormald, *Journal of Applied Probability* **36**, 999 (1999).
- [31] Y. V. Fyodorov, A. Ossipov, and A. Rodriguez, *Journal of Statistical Mechanics: Theory and Experiment* **2009**, L12001 (2009).
- [32] E. Bogomolny and O. Giraud, *Phys. Rev. E* **85**, 046208 (2012).
- [33] V. E. Kravtsov, I. M. Khaymovich, E. Cuevas, and M. Amini, *New Journal of Physics* **17**, 122002 (2015).
- [34] C. H. Lee, D. Ozaki, and H. Matsueda, *Phys. Rev. E* **94**, 062144 (2016).
- [35] K. Truong and A. Ossipov, *Journal of Physics A: Mathematical and Theoretical* **51**, 065001 (2018).
- [36] A. Bäcker, M. Haque, and I. M. Khaymovich, *Phys. Rev. E* **100**, 032117 (2019).
- [37] K. S. Tikhonov and A. D. Mirlin, *Phys. Rev. B* **99**, 024202 (2019).
- [38] A. I. Olemskoï and A. Y. Flat, *Physics-Uspexhi* **36**, 1087 (1993).
- [39] T. Nakayama, “Fractal structures in condensed matter physics,” in *Encyclopedia of Complexity and Systems Science* (Springer New York, New York, NY, 2009) pp. 3878–3893.
- [40] X. Deng, B. L. Altshuler, G. V. Shlyapnikov, and L. Santos, *Phys. Rev. Lett.* **117**, 020401 (2016).
- [41] T. Banks, L. Susskind, and J. Kogut, *Phys. Rev. D* **13**, 1043 (1976).
- [42] J. Kogut and L. Susskind, *Phys. Rev. D* **11**, 395 (1975).
- [43] P. Jordan and E. Wigner, *Zeitschrift für Physik* **47**, 631 (1928).
- [44] M. Joshi, A. K. Agarwal, and B. Gupta, in *Soft Computing: Theories and Applications*, edited by K. Ray, T. K. Sharma, S. Rawat, R. K. Saini, and A. Bandyopadhyay (Springer Singapore, Singapore, 2019) pp. 235–243.
- [45] P. Vigier, “fractal-image-compression,” <https://github.com/pvigier/fractal-image-compression> (2019).
- [46] S. Coleman, *Annals of Physics* **101**, 239 (1976).
- [47] T. M. R. Byrnes, P. Sriganesh, R. J. Bursill, and C. J. Hamer, *Phys. Rev. D* **66**, 013002 (2002).
- [48] L. Funcke, K. Jansen, and S. Kühn, *Phys. Rev. D* **101**, 054507 (2020).
- [49] C. Kokail, C. Maier, R. van Bijnen, T. Brydges, M. K. Joshi, P. Jurcevic, C. A. Muschik, P. Silvi, R. Blatt, C. F. Roos, and P. Zoller, *Nature* **569**, 355 (2019).
- [50] O. V. Borzenkova, G. I. Struchalin, A. S. Kardashin, V. V. Krasnikov, N. N. Skryabin, S. S. Straupe, S. P. Kulik, and J. D. Biamonte, *Applied Physics Letters* **118**, 144002 (2021), <https://doi.org/10.1063/5.0043322>.
- [51] T. Brydges, A. Elben, P. Jurcevic, B. Vermersch, C. Maier, B. P. Lanyon, P. Zoller, R. Blatt, and C. F. Roos, *Science* **364**, 260 (2019), <https://www.science.org/doi/pdf/10.1126/science.aau4963>.
- [52] B. Yoshida, *Phys. Rev. B* **88**, 125122 (2013).
- [53] J. I. Latorre, “Image compression and entanglement,” (2005), [arXiv:quant-ph/0510031](https://arxiv.org/abs/quant-ph/0510031) [quant-ph].
- [54] I. Glasser, N. Pancotti, M. August, I. D. Rodriguez, and J. I. Cirac, *Phys. Rev. X* **8**, 011006 (2018).

SUPPLEMENTARY INFORMATION

S1. ANSATZ

Here we explain in details how we use fractal structure to obtain distributions and find energies. We use several levels of approximation for our calculations. The first level is given by the following 4-term ansatz:

$$|\Psi_N^A\rangle = W_{0011} |0011\rangle |\Psi_{N-4}\rangle + W_{01} |01\rangle |\Psi_{N-2}\rangle + W_{10} |10\rangle |\Psi_{N-2}\rangle + W_{110} |110\rangle \hat{T} |\Psi_{N-3}\rangle. \quad (\text{S1})$$

where $\hat{T} = \otimes_k \hat{\sigma}_k^x$ is the bit flipping operator.

The second level of approximation can be presented as following:

$$|\Psi_N^A\rangle = W_{001011} |001011\rangle |\Psi_{N-6}\rangle + W_{0011} |0011\rangle |\Psi_{N-4}\rangle + W_{01} |01\rangle |\Psi_{N-2}\rangle + W_{10} |10\rangle |\Psi_{N-2}\rangle + \\ + W_{110} |110\rangle \hat{T} |\Psi_{N-3}\rangle + W_{11100} |11100\rangle \hat{T} |\Psi_{N-5}\rangle. \quad (\text{S2})$$

To obtain more accurate distribution, we add terms with GS for $N - 6$ and $N - 5$ number of sites. Then, we use the following 9-term fractal ansatz:

$$|\Psi_N^A\rangle = W_{001011} |001011\rangle |\Psi_{N-6}\rangle + W_{0011} |0011\rangle |\Psi_{N-4}\rangle + W_{01} |01\rangle |\Psi_{N-2}\rangle + \\ + |10\rangle (W_{100011} |0011\rangle |\Psi_{N-6}\rangle + W_{1001} |01\rangle |\Psi_{N-4}\rangle + W_{1010} |10\rangle |\Psi_{N-4}\rangle + W_{10110} |110\rangle \hat{T} |\Psi_{N-5}\rangle) + \\ + W_{110} |110\rangle \hat{T} |\Psi_{N-3}\rangle + W_{11100} |11100\rangle \hat{T} |\Psi_{N-5}\rangle, \quad (\text{S3})$$

$P_{10} |\Psi\rangle$ part is not perfectly fits the wave function for $N - 2$ spins, that is why we divide it into four parts. To include more amplitudes, we propose the 11-term fractal ansatz:

$$|\Psi_N^A\rangle = W_{001011} |001011\rangle |\Psi_{N-6}\rangle + W_{0011} |0011\rangle |\Psi_{N-4}\rangle + W_{01} |01\rangle |\Psi_{N-2}\rangle - \\ + |10\rangle (W_{10001011} |001011\rangle |\Psi_{N-8}\rangle + W_{100011} |0011\rangle |\Psi_{N-6}\rangle + W_{1001} |01\rangle |\Psi_{N-4}\rangle + \\ + W_{1010} |10\rangle |\Psi_{N-4}\rangle + W_{10110} |110\rangle \hat{T} |\Psi_{N-5}\rangle + W_{1011100} |11100\rangle \hat{T} |\Psi_{N-7}\rangle) + \\ + W_{110} |110\rangle \hat{T} |\Psi_{N-3}\rangle + W_{11100} |11100\rangle \hat{T} |\Psi_{N-5}\rangle. \quad (\text{S4})$$

Here more parts in $P_{10} |\Psi\rangle$ sector are added, so the 11-term ansatz includes 9-term.

For ansatz diagonalization method we build Hamiltonian in corresponding basis. Nonzero elements of the reduced Hamiltonian for ansatz (S2) are as follows:

$$\begin{aligned} H_{1,1} &= E_{N-6} + 5 + 2\mu, & H_{2,2} &= E_{N-4} + 3 + 2\mu, \\ H_{3,3} &= E_{N-2} + 1 + 2\mu, & H_{4,4} &= E_{N-4}, \\ H_{5,5} &= E_{N-3} + 1 + 2\mu, & H_{6,6} &= E_{N-5} + 3 + 2\mu, \\ H_{1,2} &= \langle 001011\Psi_{N-6} | \hat{H} | 0011\Psi_{N-4} \rangle = xW_{01}^{N-4}, \\ H_{1,3} &= \langle 001011\Psi_{N-6} | \hat{H} | 01\Psi_{N-2} \rangle = xW_{0011}^{N-2}, \\ H_{2,3} &= \langle 0011\Psi_{N-4} | \hat{H} | 01\Psi_{N-2} \rangle = xW_{0011}^{N-2}, \\ H_{3,4} &= \langle 01\Psi_{N-2} | \hat{H} | 10\Psi_{N-2} \rangle = x, \\ H_{4,5} &= \langle 10\Psi_{N-2} | \hat{H} | 110\hat{T}\Psi_{N-3} \rangle = xf_{N-2}, \\ H_{5,6} &= \langle 110\hat{T}\Psi_{N-3} | \hat{H} | 11100\hat{T}\Psi_{N-5} \rangle = xW_{01}^{N-3}, \\ f_{N-2} &= x(W_{10}^{N-2}(W_{10}^{N-3}f_{N-4} + W_{110}^{N-3}W_{01}^{N-4} + W_{110}^{N-2}W_{11100}^{N-4}) + W_{11100}^{N-2}W_{0011}^{N-3}). \end{aligned} \quad (\text{S5})$$

Rest elements in the reduced Hamiltonian are zero.

The reduced Hamiltonian for the 11-term ansatz is the following:

$$\begin{aligned} H_{4,4} &= E_{N-8} + 5 + 2\mu, & H_{5,5} &= E_{N-6} + 3 + 2\mu, \\ H_{6,6} &= E_{N-4} + 1 + 2\mu, & H_{7,7} &= E_{N-4}, \\ H_{8,8} &= E_{N-5} + 1 + 2\mu, & H_{9,9} &= E_{N-7} + 3 + 2\mu. \end{aligned} \quad (\text{S6})$$

The following elements replace $H_{3,4}$ and $H_{4,5}$:

$$\begin{aligned}
H_{3,4} &= \langle 01\Psi_{N-2}|H|10001011\Psi_{N-8}\rangle = xW_{001011}^{N-2}, \\
H_{3,5} &= \langle 01\Psi_{N-2}|H|100011\Psi_{N-6}\rangle = xW_{0011}^{N-2}, \\
H_{3,6} &= \langle 01\Psi_{N-2}|H|10001\Psi_{N-4}\rangle = xW_{01}^{N-2}, \\
H_{3,7} &= \langle 01\Psi_{N-2}|H|1010\Psi_{N-8}\rangle = xW_{10}^{N-2} = g_{N-2}, \\
H_{3,8} &= \langle 01\Psi_{N-2}|H|10110\Psi_{N-5}\rangle = xW_{110}^{N-2}, \\
H_{3,9} &= \langle 01\Psi_{N-2}|H|1011100\Psi_{N-7}\rangle = xW_{11100}^{N-2}, \\
H_{7,10} &= \langle 1010\Psi_{N-4}|\hat{H}|110\hat{T}\Psi_{N-3}\rangle = f_{N-3}, \\
H_{8,10} &= \langle 10110\hat{T}\Psi_{N-5}|\hat{H}|110\hat{T}\Psi_{N-3}\rangle = xW_{01}^{N-2}, \\
H_{9,10} &= \langle 1011100\hat{T}\Psi_{N-7}|\hat{H}|110\hat{T}\Psi_{N-3}\rangle = xW_{0011}^{N-3}, \\
H_{4,5} &= \langle 10001011\Psi_{N-8}|H|100011\Psi_{N-6}\rangle = xW_{01}^{N-6}, \\
H_{4,6} &= \langle 10001011\Psi_{N-8}|H|1001\Psi_{N-4}\rangle = xW_{0011}^{N-4}, \\
H_{8,9} &= \langle 10110\hat{T}\Psi_{N-5}|H|1011100\hat{T}\Psi_{N-7}\rangle = xW_{01}^{N-5} \\
g_N &= \langle 10\Psi_{N-2}|\Psi_N\rangle = W_{10001011}^N W_{001011}^{N-2} + W_{100011}^N W_{0011}^{N-2} \\
&+ W_{1001}^N W_{01}^{N-2} + W_{1010}g_{N-2} + W_{10110}^N W_{110}^{N-2} + W_{1011100}^N W_{11100}^N, \\
f_N &= W_{100011}^N W_{11100}^{N-1} + W_{1001}^N W_{110}^{N-1} + W_{1010}p_{N-1} + \\
&+ W_{10110}^N W_{1001}^{N-1} + W_{1011100}^N W_{100011}^{N-1} + W_{110}^N W_{01}^{N-1} + W_{11100}^N W_{0011}^{N-1}, \\
p_N &= \langle \Psi_N|101\hat{T}\Psi_{N-3}\rangle = W_{1010}^N f_{N-3} + W_{10110}^N W_{01}^{N-3} + W_{1011100}^N W_{0011}^{N-3}.
\end{aligned} \tag{S7}$$

Elements $H_{1,1}$, $H_{2,2}$, $H_{3,3}$, $H_{1,2}$, $H_{1,3}$, and $H_{2,3}$ are the same as for matrix (S5). Elements $H_{10,11}$, $H_{10,10}$, $H_{11,11}$ of matrix (S7) are equal to the elements $H_{5,6}$, $H_{5,5}$, $H_{6,6}$ of matrix (S5).

The mean energy in terms of ansatz (S3) that is used in the AWF method reads

$$\begin{aligned}
E_N &= W_{001011}^2(E_{N-6} + 5 + 2\mu) + W_{0011}^2(E_{N-4} + 3 + 2\mu) + W_{01}^2(E_{N-2} + 1 + 2\mu) + \\
&(W_{100011}^2(E_{N-6} + 3 + 2\mu) + W_{1001}^2(E_{N-4} + 1 + 2\mu) + W_{1010}^2(E_{N-4}) + W_{10110}^2(E_{N-5} + 1 + 2\mu)) + \\
&W_{110}^2(E_{N-3} + 1 + 2\mu) + W_{11000}^2(E_{N-5} + 3 + 2\mu) + 2C.
\end{aligned} \tag{S8}$$

For ansatz (S4) the energy takes the following form:

$$\begin{aligned}
E_N &= W_{001011}^2(E_{N-6} + 5 + 2\mu) + W_{0011}^2(E_{N-4} + 3 + 2\mu) + W_{01}^2(E_{N-2} + 1 + 2\mu) + \\
&(W_{10001011}^2(E_{N-8} + 5 + 2\mu) + W_{100011}^2(E_{N-6} + 3 + 2\mu) + W_{1001}^2(E_{N-4} + 1 + 2\mu) + W_{1010}^2(E_{N-4}) + \\
&+ W_{10110}^2(E_{N-5} + 1 + 2\mu) + W_{1011100}^2(E_{N-7} + 3 + 2\mu)) + W_{110}^2(E_{N-3} + 1 + 2\mu) + W_{11000}^2(E_{N-5} + 3 + 2\mu) + 2C'.
\end{aligned} \tag{S9}$$

Where C comes from the average of hopping term term and has the following form:

$$\begin{aligned}
C &= W_{001011}W_{01} \langle 001011\Psi_{N-6}|\hat{H}|01\Psi_{N-2}\rangle + W_{001011}W_{0011} \langle 001011\Psi_{N-6}|\hat{H}|0011\Psi_{N-4}\rangle + \\
&+ W_{0011}W_{01} \langle 0011\Psi_{N-4}|\hat{H}|01\Psi_{N-2}\rangle + W_{01}W_{100011} \langle 01\Psi_{N-2}|\hat{H}|100011\Psi_{N-6}\rangle + \\
&+ W_{01}W_{1001} \langle 01\Psi_{N-2}|\hat{H}|1001\Psi_{N-4}\rangle + W_{01}W_{1010} \langle 01\Psi_{N-2}|\hat{H}|1010\Psi_{N-4}\rangle + \\
&+ W_{01}W_{10110} \langle 01\Psi_{N-2}|\hat{H}|10110\hat{T}\Psi_{N-5}\rangle + W_{1001}W_{100011} \langle 100011\Psi_{N-6}|\hat{H}|1001\Psi_{N-4}\rangle \\
&+ W_{1010}W_{10110} \langle 1010\Psi_{N-4}|\hat{H}|10110\hat{T}\Psi_{N-5}\rangle + W_{110}W_{1010} \langle 110\hat{T}\Psi_{N-3}|\hat{H}|1010\Psi_{N-4}\rangle + \\
&+ W_{110}W_{10110} \langle 110\hat{T}\Psi_{N-3}|\hat{H}|10110\hat{T}\Psi_{N-5}\rangle + W_{001011}W_{0011} \langle 001011\Psi_{N-6}|\hat{H}|0011\Psi_{N-4}\rangle + \\
&+ W_{001011}W_{01} \langle 001011\Psi_{N-6}|\hat{H}|01\Psi_{N-2}\rangle + W_{11100}W_{110} \langle 11100\hat{T}\Psi_{N-5}|\hat{H}|110\hat{T}\Psi_{N-3}\rangle + \\
&+ W_{1001}W_{1010} \langle 1001\Psi_{N-4}|1010\Psi_{N-4}\rangle.
\end{aligned} \tag{S10}$$

Eq. (S10) can be further simplified, knowing that \hat{H} acts on these states by flipping only neighbouring spins. Thus,

C can be written down in terms of overlaps

$$\begin{aligned}
C/x = & W_{001011}W_{01} \langle 0011\Psi_{N-6}|\Psi_{N-2} \rangle + W_{001011}W_{0011} \langle 01\Psi_{N-6}|\Psi_{N-4} \rangle + \\
& + W_{0011}W_{01} \langle \Psi_{N-2}|01\Psi_{N-4} \rangle + W_{01}W_{100011} \langle \Psi_{N-2}|0011\Psi_{N-6} \rangle + \\
& + W_{01}W_{1001} \langle \Psi_{N-2}|01\Psi_{N-4} \rangle + W_{01}W_{1010} \langle \Psi_{N-2}|10\Psi_{N-4} \rangle + \\
& + W_{01}W_{10110} \langle \Psi_{N-2}|110\hat{T}\Psi_{N-5} \rangle + W_{1001}W_{100011} \langle 01\Psi_{N-6}|\Psi_{N-4} \rangle \\
& + W_{1010}W_{10110} \langle \Psi_{N-4}|1\hat{T}\Psi_{N-5} \rangle + W_{110}W_{1010} \langle \hat{T}\Psi_{N-3}|0\Psi_{N-4} \rangle + \\
& + W_{110}W_{10110} \langle \hat{T}\Psi_{N-3}|10\hat{T}\Psi_{N-5} \rangle + W_{001011}W_{0011} \langle 01\Psi_{N-6}|\Psi_{N-4} \rangle + \\
& + W_{001011}W_{01} \langle \Psi_{N-2}|0011\Psi_{N-6} \rangle + W_{11100}W_{110} \langle \hat{T}\Psi_{N-3}|10\hat{T}\Psi_{N-5} \rangle + \\
& + W_{1001}W_{1010}.
\end{aligned} \tag{S11}$$

$$\begin{aligned}
C'/x = & C/x + W_{10001011}W_{100011} \langle 01\Psi_{N-8}|\Psi_{N-6} \rangle + W_{10001011}W_{1001} \langle 0011\Psi_{N-8}|\Psi_{N-4} \rangle + \\
& + W_{10110}W_{1011100} \langle \hat{T}\Psi_{N-5}|10\hat{T}\Psi_{N-7} \rangle + W_{10}W_{10001011} \langle \Psi_{N-2}|001011\Psi_{N-8} \rangle + \\
& + W_{01}W_{1011100} \langle \Psi_{N-2}|11100\hat{T}\Psi_{N-7} \rangle + W_{1011100}W_{110} \langle 1100\hat{T}\Psi_{N-7}|\hat{T}\Psi_{N-3} \rangle.
\end{aligned} \tag{S12}$$

Using this formula, we can recursively calculate energy for arbitrary numbers of qubits.

S2. WEIGHTS

Here we present the absolute values of weights for different parameters x and μ and number of sites obtained by MPS calculations, see Fig. S1. Weights are required in our approach for calculating wave functions and energies. One can see that weights become constants with the system size. This convergence is essential for the validity of the self-similar approach.

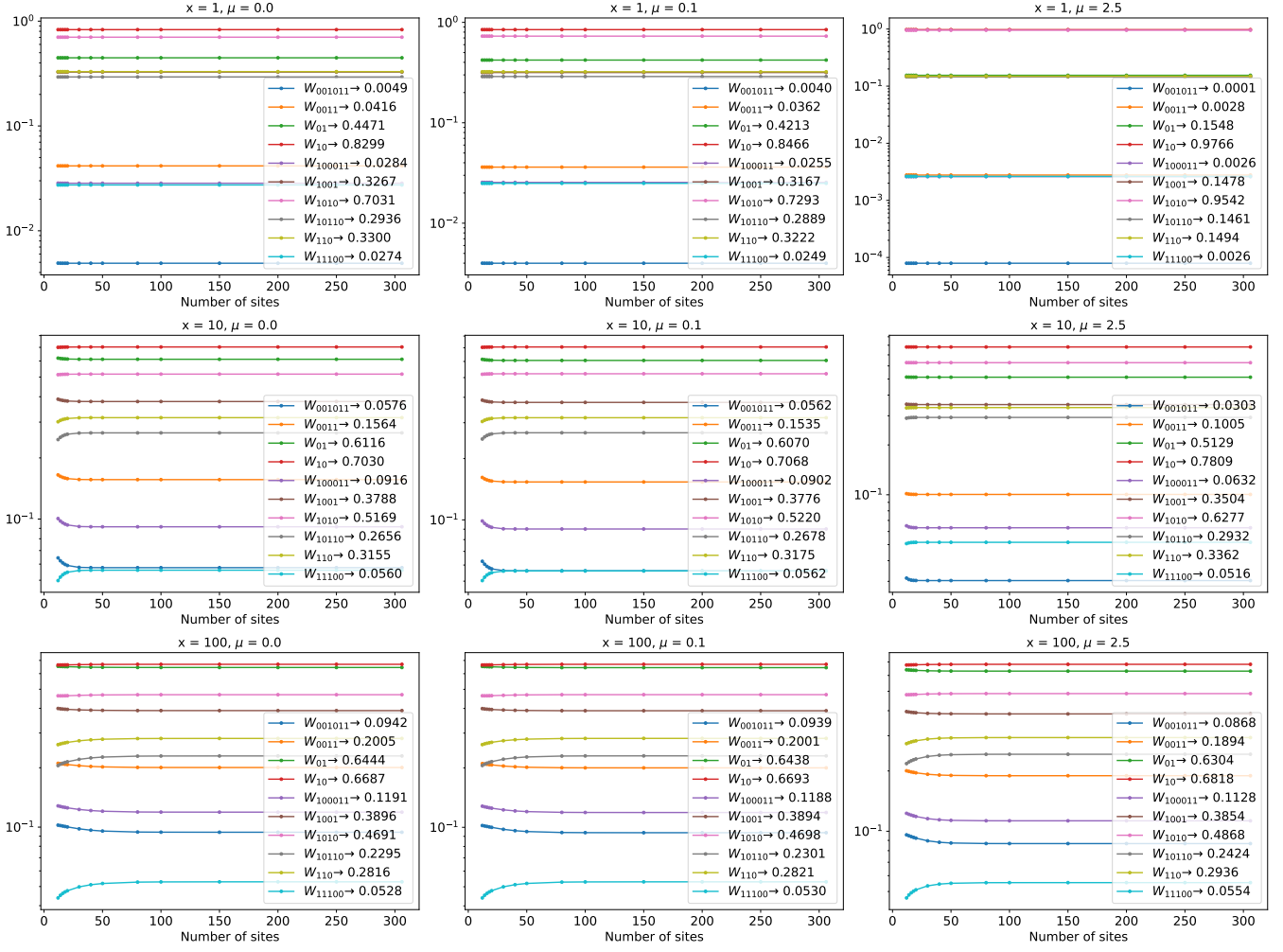


Figure S1. MPS calculations of weights for different parts of the wave function and various parameters of the Hamiltonian.

S3. ERRORS

The errors occurred in algorithm comes from the two ways. First of all, we neglect some amplitudes using fractal ansatzes. Secondly, we simplify the structure of the wave function assuming it to be made of exactly the distributions for previous dimensions. First type of errors can be easily calculated. In Fig. S2 we illustrate the amount of neglected probability for different parameters and different ansatzes.

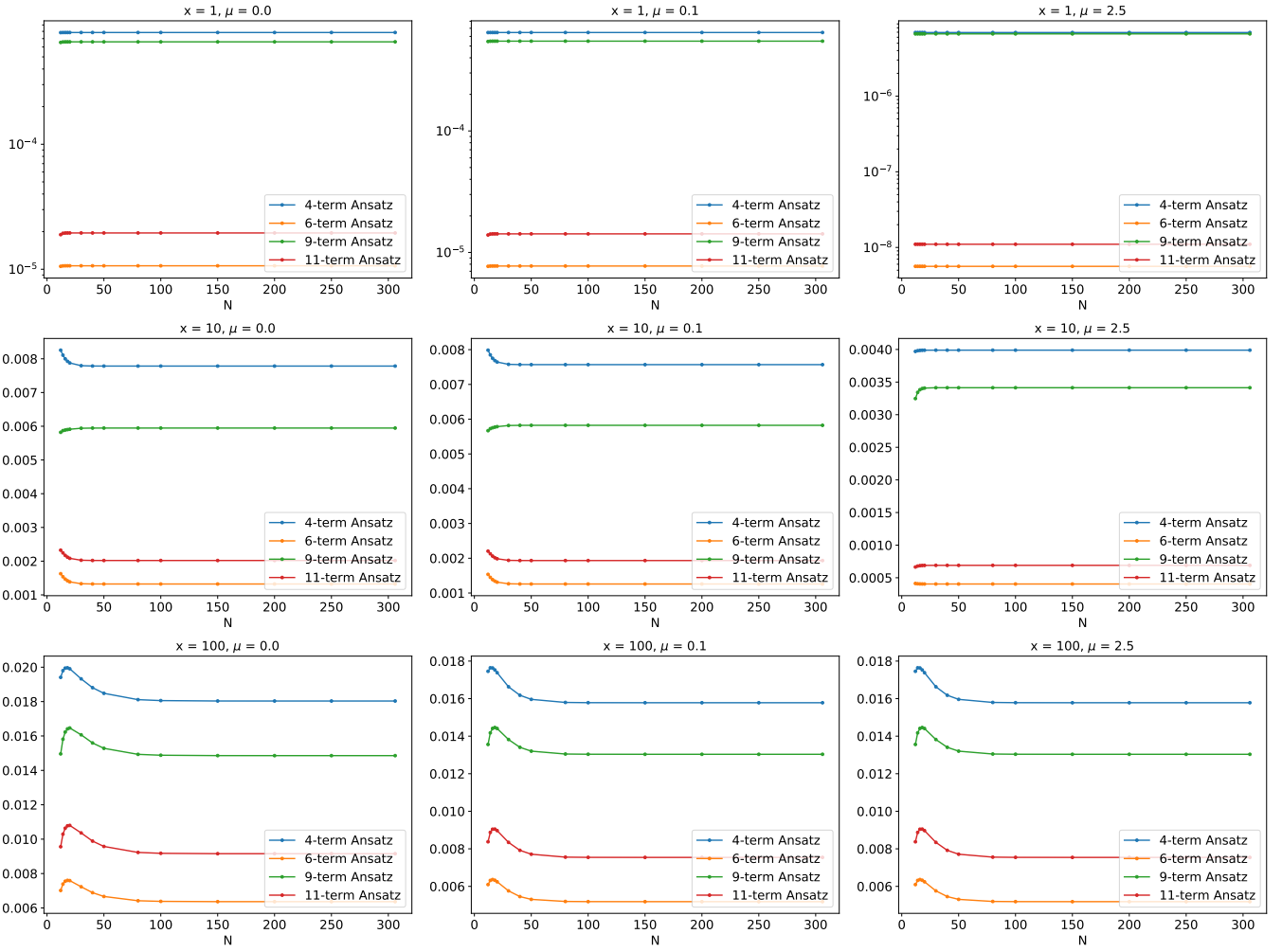


Figure S2. The figure represents neglected probabilities for different parameters and different ansatzes. Neglected probabilities are equal to the $1 - \sum_i W_i^2$ where W_i is a weight.

S4. DIFFERENT BASES

Fractal structure exists in different bases. The fractal structure is unique in each basis. It can be easily seen in qubism representation, see Fig. S3.

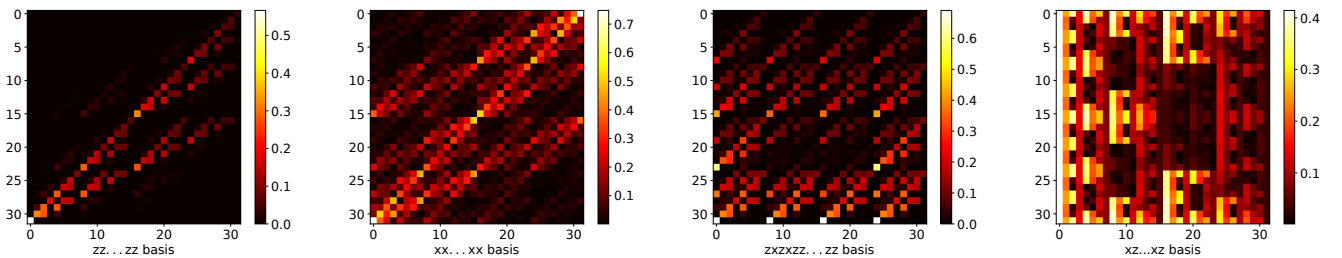


Figure S3. Probability distributions in different bases, which clearly indicate on the presence of the fractal structure.